Journal of Zhejiang University-SCIENCE A (Applied Physics & Engineering) 2023 24(8):735-748
www.jzus.zju.edu.cn; www.springer.com/journal/11582
E-mail: jzus_a@zju.edu.cn

Research Article

https://doi.org/10.1631/jzus.A2200625

Effects of potassium channel blockage on inverse stochastic resonance in Hodgkin-Huxley neural systems

Xueqing WANG, Dong YU, Yong WU, Qianming DING, Tianyu LI, Ya JIA✉

Department of Physics, Central China Normal University, Wuhan 430079, China

Abstract: Inverse stochastic resonance (ISR) is a phenomenon in which the firing activity of a neuron is inhibited at a certain noise level. In this paper, the effects of potassium channel blockage on ISR in single Hodgkin-Huxley neurons and in small-world networks were investigated. For the single neuron, the ion channel noise-induced ISR phenomenon can occur only in a certain small range of potassium channel blockage ratio. Bifurcation analysis showed that this small range is the bistable region regulated by the external bias current. For small-world networks, the effect of non-homogeneous network blockage on ISR was investigated. The network blockage ratio was used to represent the proportion of potassium-channel-blocked neurons to total network neurons. It is found that an increase in network blockage ratio at small coupling strengths results in shorter ISR duration. When the coupling strength is increased, the ISR is more significant in the case of a large network blockage ratio. The ISR phenomenon is determined by the network blockage ratio, the coupling strength, and the ion channel noise. Our results will provide new perspectives on the observation of ISR in neuroscience experiments.

Key words: Inverse stochastic resonance (ISR); Small-world neuronal network; Potassium channel blockage; Network blockage ratio

1 Introduction

It was widely believed that adding noise (Faisal et al., 2008; Jin et al., 2019; Yu et al., 2021, 2022a) to the transmission of information by neurons (Ma, 2023) tended to have a negative effect. However, a counter-intuitive effect (stochastic resonance) (Liu and Li, 2013) allows the non-linear system to obtain the maximum response to the signal at the appropriate noise level (Gluckman et al., 1996; Gailey et al., 1997; Perc, 2007; Wang et al., 2009; Kawaguchi et al., 2011). This means that proper noise can improve the efficiency of information transmission and processing by amplifying the neuron's response to the signal (Chik et al., 2001; Kosko and Mitaim, 2003; McDonnell and Abbott, 2009). In addition, noise has an inhibitory effect on neuronal activity. In experiments on the in-vitro preparation of squid axons, Paydarfar et al. (2006) found that small noise could inhibit neuronal pacemaker activity and induce switching behaviour between repetitive firing and resting. Gutkin et al. (2009) and Tuckwell et al. (2009) studied the role of noise on the firing rhythms of Hodgkin-Huxley (HH) neurons (Hodgkin and Huxley, 1952a). The results showed that a minimum of neuronal firing activity occurred at moderate noise levels. This phenomenon is referred to as inverse stochastic resonance (ISR).

In recent years, ISR has been extensively researched and proved both experimentally and theoretically. On one hand, Buchin et al. (2016) found that a noise of specific amplitude in cerebellar Purkinje cells can effectively suppress spike generation, thus providing the primary experimental evidence for ISR. Huh (2016) reported that ISR can be observed in alternating current-driven electrical convection in nematic liquid crystals. On the other hand, Uzuntarla et al. (2013) investigated channel noise-induced ISR in HH neurons, demonstrating that ISR depends on the setting of the initialization time in the simulation. They also elucidated the mechanism behind ISR from the perspective of kinetic structure. Furthermore, the ISR with specific biophysical mechanisms was discussed. It was

✉ Ya JIA, jiay@ccnu.edu.cn
Ya JIA, https://orcid.org/0000-0002-2818-9074

Received Dec. 29, 2022; Revision accepted Mar. 30, 2023;
Crosschecked June 20, 2023; Online first Aug. 3, 2023

found that ISR is related to synaptic input mechanisms (Uzuntarla, 2013), and ISR is most significant when excitatory and inhibitory synaptic currents are in relative balance. Further, the authors reported on the dual ISR (Uzuntarla et al., 2017a) induced by dynamic synapses and the more complex kinetic mechanisms behind it. In addition to ISR induced by ion channel noise, other noises can also induce ISR effects. It is found that Gaussian colored noise (Lu et al., 2020), non-Gaussian colored noise (Li et al., 2018), and Levy noise (Zhao and Li, 2019; Li et al., 2020) can also induce ISR effects (Wang et al., 2022). ISR has been further extended to neuronal networks (Uzuntarla et al., 2017b).

During the generation of action potentials in neurons (Wu et al., 2018; Zhang and Ma, 2021; Yu et al., 2022b, 2023a, 2023b), the distribution of ion channels is one of the important influencing factors. Tetraethylammonium (TEA) and tetrodotoxin (TTX) can reduce the numbers of open potassium channels and sodium channels, respectively (Narahashi and Moore, 1968; Hoyt and Strieb, 1971). Schmid et al. (2004) investigated the effect of ion channel blockage on neuronal excitability in stochastic HH neurons. Their results showed that very small amounts of TTX lead to a decrease in action potentials and irregular peak activity. In contrast, small amounts of TEA increased the amount and regularity of peak activity. In addition to affecting neuronal excitability by reducing the number of open ion channels, toxins can also affect membrane potential by causing a decrease in conductance (Goldwyn et al., 2011; Ma et al., 2011; Liu et al., 2013; Xu et al., 2018, 2019). In the past, when poisoning was considered in a neuronal network, the neurons in it were generally considered to be uniformly poisoned. In other words, all neuronal ion channels in the network were poisoned simultaneously and to the same extent. However, due to the variability of single neurons and the fact that neural tissue is generally anisotropic, toxins might cause localized poisoning at different locations, i.e., the poisoning was non-uniform. Neural networks with random channel poisoning have a richer dynamical behavior than those with uniform channel poisoning (Wu et al., 2013a). Moreover, the stochastic nature of ion channel gating may lead both to threshold fluctuations in neurons and also be a major source of ion channel noise generation (White et al., 2000; Maisel and Lindenberg, 2020; Ding and Jia, 2021).

In previous studies, although ISR induced by ion channel noise in HH neurons has been considered (Uzuntarla et al., 2013), to our knowledge the effects of potassium channel blockage on ISR have not received much attention. Therefore, some interesting questions arise: How does potassium channel blockage affect the ISR in neurons? Does the ISR in a network change when drugs block neurons in the network unevenly? How do interactions between neurons affect the ISR?

In this paper we investigate the effects of potassium ion channel blockage as well as external bias currents on the ISR of single HH neurons and explore the ISR effects in small-world networks. The HH neuron model and neural network containing ion channel blockage are introduced, and ISR effects in single neurons and neuronal networks are discussed.

2 Models and methods

The kinetic equation for the change in membrane potential over time t in HH neurons containing blocked ion channels is as follows (Hodgkin and Huxley, 1952b):

$$C\frac{\mathrm{d}V}{\mathrm{d}t}=-G_{\mathrm{K}}x_{\mathrm{K}}n^4(V-E_{\mathrm{K}})-G_{\mathrm{Na}}x_{\mathrm{Na}}m^3h(V-E_{\mathrm{Na}})-G_{\mathrm{L}}(V-E_{\mathrm{L}})+I_{\mathrm{ext}}, \tag{1}$$

where V is the membrane potential of the neuron and C= 1 μF/cm^2 is the membrane capacitance. G_{K}=36 mS/cm^2, G_{Na}=120 mS/cm^2, and G_{L}=0.3 mS/cm^2 indicate the maximum conductance of potassium, sodium, and leakage currents, respectively. x_{K} indicates the ratio of non-blocking potassium channels to total potassium channels, and x_{Na} is the ratio of non-blocking sodium channels to total sodium channels. Thus, ion channel blockage ratios x_{K} and x_{Na} are negatively correlated with the degree of blockage. At resting potential, the cell membrane is much more permeable to potassium ions than to sodium ions, so blockage of sodium channels has little effect on the resting potential of neurons (Schmid et al., 2004; Lu et al., 2017; Xu et al., 2018; Liu et al., 2019). In the present study, we focus on the effect of potassium channel blockage and the sodium channel blockage ratio is fixed as x_{Na}=1.0. The parameters E_{K}= −77 mV, E_{Na}=50 mV, and E_{L}=−54.4 mV are the reversal potentials for potassium, sodium, and leakage currents,

respectively. In addition, I_{ext} is the external bias current that can modulate neuronal excitability.

In Eq (1), n is the activation gating variable of the potassium ion channel, and m and h represent the activation and deactivation gating variables for sodium channels in neurons, respectively. Considering ion channel noise in the dynamical behavior of neurons, the Fox algorithm is used (Fox, 1997), where the gating variables obey the following Langevin equation:

$$\frac{\mathrm{d}y}{\mathrm{d}t}=\alpha_y(1-y)-\beta_y y+\xi_y(t),\ y=n,\ m,\ h, \tag{2}$$

where α_y and β_y are voltage-dependent rate functions of the gating variable y (y=n, m, h) described as follows:

$$\begin{cases}\alpha_n=\dfrac{0.01(V+55)}{1-\exp[-(V+55)/10]},\\ \beta_n=0.125\exp[-(V+65)/80],\\ \alpha_m=\dfrac{0.1(V+40)}{1-\exp[-(V+40)/10]},\\ \beta_m=4\exp[-(V+65)/18],\\ \alpha_h=0.07\exp[-(V+65)/20],\\ \beta_h=\left\{1+\exp[-(V+35)/10]\right\}^{-1},\end{cases} \tag{3}$$

and the random variable $\xi_y(t)$ is an independent zero-mean Gaussian white noise whose autocorrelation function satisfies the following equations:

$$\begin{cases}\langle\xi_n(t)\,\xi_n(t')\rangle=\dfrac{2}{N_{\mathrm{K}}x_{\mathrm{K}}}\dfrac{\alpha_n\beta_n}{\alpha_n+\beta_n}\delta(t-t'),\\ \langle\xi_m(t)\,\xi_m(t')\rangle=\dfrac{2}{N_{\mathrm{Na}}x_{\mathrm{Na}}}\dfrac{\alpha_m\beta_m}{\alpha_m+\beta_m}\delta(t-t'),\\ \langle\xi_h(t)\,\xi_h(t')\rangle=\dfrac{2}{N_{\mathrm{Na}}x_{\mathrm{Na}}}\dfrac{\alpha_h\beta_h}{\alpha_h+\beta_h}\delta(t-t').\end{cases} \tag{4}$$

In Eq (4), the total numbers of potassium and sodium ion channels in a membrane patch are given by $N_{\mathrm{K}}=\rho_{\mathrm{K}}\times S$ and $N_{\mathrm{Na}}=\rho_{\mathrm{Na}}\times S$, respectively, where S indicates the membrane area. Assuming homogeneous density of ion channels, the potassium and sodium ion channel densities are ρ_{K}=18 μm^{-2} and ρ_{Na}=60 μm^{-2}, respectively. From a statistical physics point of view, the intensity of ion channel noise $\xi(t)$ decreases with increasing S. Throughout the study, the membrane area S will be used as the control parameter for channel noise.

In neuronal networks, the kinetic equations of the network are as follows:

$$\begin{aligned}C\frac{\mathrm{d}V_i}{\mathrm{d}t}&=-G_{\mathrm{K}}x_{\mathrm{K},i}n_i^4(V_i-E_{\mathrm{K}})-G_{\mathrm{Na}}x_{\mathrm{Na},i}m_i^3h_i\times\\ &\quad(V_i-E_{\mathrm{Na}})-G_{\mathrm{L}}(V_i-E_{\mathrm{L}})+I_{\mathrm{ext}}+I_i^{\mathrm{syn}},\\ \frac{\mathrm{d}y_i}{\mathrm{d}t}&=\alpha_{y,i}(1-y_i)-\beta_{y,i}y_i+\xi_{y,i}(t),\quad y=n,\ m,\ h,\end{aligned} \tag{5}$$

and the autocorrelation function for Gaussian white noise in the network is as follows:

$$\begin{cases}\left\langle\xi_{n,i}(t)\,\xi_{n,i}(t')\right\rangle=\dfrac{2}{N_{\mathrm{K}}x_{\mathrm{K},i}}\dfrac{\alpha_{n,i}\beta_{n,i}}{\alpha_{n,i}+\beta_{n,i}}\delta(t-t'),\\ \left\langle\xi_{m,i}(t)\,\xi_{m,i}(t')\right\rangle=\dfrac{2}{N_{\mathrm{Na}}x_{\mathrm{Na},i}}\dfrac{\alpha_{m,i}\beta_{m,i}}{\alpha_{m,i}+\beta_{m,i}}\delta(t-t'),\\ \left\langle\xi_{h,i}(t)\,\xi_{h,i}(t')\right\rangle=\dfrac{2}{N_{\mathrm{Na}}x_{\mathrm{Na},i}}\dfrac{\alpha_{h,i}\beta_{h,i}}{\alpha_{h,i}+\beta_{h,i}}\delta(t-t').\end{cases} \tag{6}$$

In Eq (5), I_i^{syn} indicates the synaptic current of neuron i. The connections between neurons in the network are electrical synapses, where the synaptic current of neuron i is given by

$$I_i^{\mathrm{syn}}=\sum\nolimits_j g_{\mathrm{e}}\varepsilon_{i,j}\left(V_j-V_i\right), \tag{7}$$

where g_{e} is the strength of the electrical coupling between interconnected neurons. If neurons i and j are connected, $\varepsilon_{i,j}$ equals 1, otherwise it is zero. The neuronal network is modeled as a small-world network (Watts and Strogatz, 1998; Uzun et al., 2017; Yu et al., 2022c), which has the following network topology parameters: the degree K=4 and the rewiring probability p=0.4. The topology of the small-world network does not change unless otherwise indicated.

In neuronal systems, ion channels in the area of the neuronal membrane can be blocked by certain drugs (Narahashi and Moore, 1968; Hoyt and Strieb, 1971). In most cases, the blockage of neuronal networks by drugs is non-uniform, so it is of significance to study the overall effect of ion channel blockage in a portion of the neuron in the network (Wu et al., 2013a, 2013b). We introduce the network blockage ratio (NBR), which represents the proportion of neurons in the network with the potassium channel blockage to the total of all neurons in the network. To simplify the study process, for blocked neurons we set the top portion of neurons, e.g., NBR=0.2, as the first 20 neurons with potassium

channel blockage (100 neurons in network). We found this network setting to be adequate for our purposes, as neurons randomly set to potassium ion blockage showed the same qualitative features as in the study here.

To investigate the ISR phenomenon in single neurons, we introduced the average firing rate of the single neurons. First, the initial conditions for the neuron were chosen randomly and uniformly in the state space (V, n, m, h), where the membrane potentials V ranged from −80 mV to 40 mV and each gating variable of n, m, and h ranged from 0 to 1. Then, after an initialization time of T_0=1 s, the number of spikes occurring in the neuron during T=10 s was recorded. Each spike is defined by a transmembrane potential above −20 mV. Therefore, the average firing rate of the neuron is calculated by

$$r=\frac{1}{HT}\left(\sum_{j=1}^{H} n_{\mathrm{spike},j}\right), \tag{8}$$

where H=100 indicates the number of times the process is repeated. This is enough repetitions for the firing rate to satisfy the statistical law. In addition, the average firing rate of the network can be calculated using the following equation:

$$R=\frac{1}{N}\left(\sum_{i=1}^{N} r_i\right), \tag{9}$$

and the number of nodes in the network is fixed at N=100. In the study of the numerical integration of this system, the fourth-order Runge-Kutta method is used with a step size of 10 μs.

3 Results

3.1 ISR in single neurons with ion channel noise

The effect of different ion channel noise and potassium channel blockage on the neuronal membrane potential is shown in Fig. 1. Looking at the left and right columns it can be seen that there is a continuous change in the membrane potential of the neuron as the membrane area increases, i.e., firing state→resting state→firing state. However, the firing of the neurons in the middle column barely changed. A horizontal comparison shows that the firing of neurons is only likely to be inhibited at moderate intensities of noise. The results show that neuronal firing is inhibited at moderate intensities of noise when potassium channel blockage is strong or weak, which indicates that the neuron undergoes ISR. However, in the case of moderate

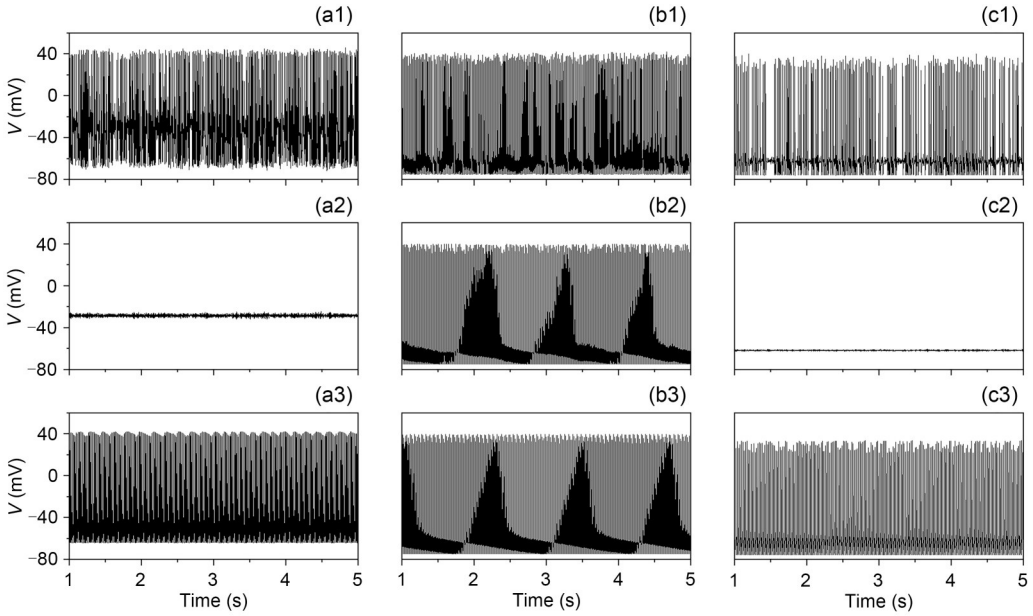

Fig. 1 Time evolution of membrane potential under conditions of different noise intensities and potassium channel blockage (I_{ext}=4.0 μA/cm^2): (a1) x_K=0.10, S=1×10^2 μm^2; (a2) x_K=0.10, S=1×10^4 μm^2; (a3) x_K=0.10, S=1×10^6 μm^2; (b1) x_K=0.50, S=1×10^2 μm^2; (b2) x_K=0.50, S=1×10^4 μm^2; (b3) x_K=0.50, S=1×10^6 μm^2; (c1) x_K=0.88, S=1×10^2 μm^2; (c2) x_K=0.88, S=1×10^4 μm^2; (c3) x_K=0.88, S=1×10^6 μm^2

potassium channel blockage, neuronal firing was barely affected by the noise.

To investigate the effect of potassium ion blockage on neuronal firing activity, the neuronal average firing rate r is plotted against the membrane area S for different x_K in Fig. 2. The observations show that for different values of x_K, different changes in the firing rate of neurons occurred. Notably, at x_K=0.09 the neuronal firing activity is diminished with decreasing noise intensity and even becomes resting. At x_K=0.20, x_K=0.30, and x_K=0.40, there is no apparent minimum in firing rate. The ISR is only observed for some specific values of x_K. To comprehensively understand the effect of x_K on the ISR effect, a contour plot of r in the S-x_K plane is shown in Fig. 3. The external bias current is fixed I_{ext}=4.0 μA/cm^2, and the blue areas indicate r=0. The results show that for 0.11<x_K<0.83, r gradually decreases, and then remains unchanged in its natural firing state. When 0.10<x_K<0.11 and 0.83<x_K<0.91, r decreases and then increases with decreasing noise intensity (increasing membrane area), i.e., the ISR effect occurs. At x_K>0.91 and x_K<0.10, the neuron gradually changes to a resting state. In other words, the ISR occurs only for a certain small range of potassium channel blockage ratios. Additionally, when the membrane area is small, the relationship between x_K and r is inverse. This means that potassium channel blockage promotes neuronal firing behaviour at appropriate noise levels. This is similar to previous results (Zhou et al., 2020).

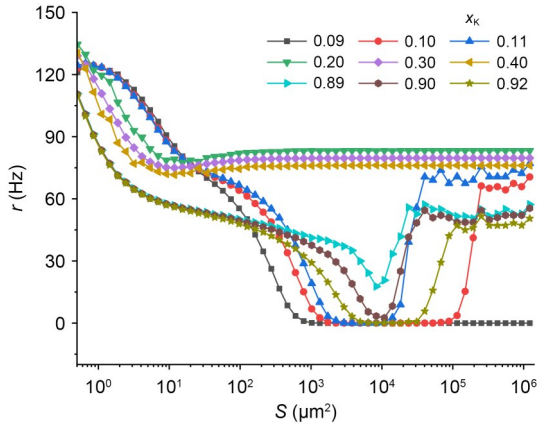

Fig. 2 Occurrence of ISR in HH neurons with different potassium channel blockages: average firing rate of neurons versus noise intensity for different potassium channel blockage conditions

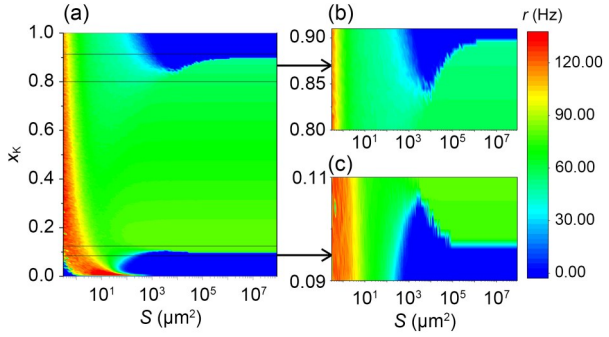

Fig. 3 Dependence of neuronal firing rate on noise intensity and potassium channel blockage (a) (I_{ext}=4.0 μA/cm^2). (b) and (c) are enlargements of the small areas in the diagram in (a). Reference to color refers to the online version of this figure

The above neuronal responses to different degrees of potassium channel blockage can be interpreted in terms of the bifurcation diagram in Fig. 4, which is the asymptotic behavior of the voltage of noise-free neurons against the potassium channel blockage ratio x_K. For x_K<x_1 and x_K>x_4, the only attractor is the stable fixed point (SFP), which means that the neurons gradually change to the resting state with decreasing noise intensity. At x_K=x_1 and x_K=x_4, the saddle-node bifurcation produces stable and unstable limit cycles (SLC and ULC). The stable limit cycles correspond to the spiking behaviour. The ULC is the boundary between the steady-state SFP and the SLC. In the bistable state, x_K has little effect on SFP and SLC, but changes the size of the ULC. The ULC converges as x_K increases for x_K∈(x_1, x_2) and as x_K decreases for x_K∈(x_3, x_4), implying

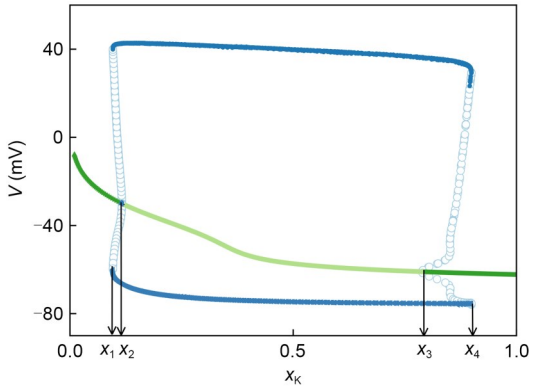

Fig. 4 Bifurcation plot of the Hodgkin-Huxley neuron model versus the ratio of potassium channel blockage x_K (from 0 to 1.0). The four critical points x_1, x_2, x_3, and x_4 are the four bifurcation points. Dark (light) green indicates stable (unstable) equilibrium, and blue solid (open) circles indicate asymptotic minima and maxima of voltage during stable (unstable) spiking behavior. Regions (x_1, x_2) and (x_3, x_4) are bistable regions. The parameter is fixed at I_{ext}=4.0 μA/cm^2. Reference to color refers to the online version of this figure

a decrease in the SFP attractor basin. This means that the neurons have difficulty transitioning from SLC to SFP, and ISR is less likely to occur. Note that SFP does not exist when $x_K \in (x_2, x_3)$, so the neuron cannot transition from the limit cycle to the non-peak state and cannot undergo ISR effects. In conclusion, ISR occurs in the bistable region corresponding to x_K, which is consistent with previous investigation (Uzuntarla et al., 2013).

The variation of the four critical points in the HH neuron model with external bias current is shown in Table 1. As I_{ext} increases, x_1 and x_2 change slightly, while x_3 and x_4 increase significantly. The results in Table 1 indicate that the external bias current can change the interval of the bistable state.

Table 1 Statistics of the four critical points at different external bias currents (Fig. 4)

I_{ext} (μA/cm^2)	x_1	x_2	x_3	x_4
0	0.086	0.107	0.549	0.636
1	0.088	0.109	0.621	0.717
2	0.091	0.112	0.684	0.786
3	0.094	0.114	0.739	0.846
4	0.096	0.116	0.789	0.899
5	0.099	0.119	0.834	0.947
6	0.102	0.121	0.874	0.990

To explore the effect of an external bias current on ISR, Fig. 5 shows the variation of neuron firing rate with noise intensity for different external bias currents. At I_{ext}=1.0 μA/cm^2 and I_{ext}=5.5 μA/cm^2, no ISR effect occurs in the neurons. The results indicate that the external bias current changes the interval of membrane area corresponding to a neuron with a firing rate of 0. Furthermore, Fig. 6 shows contour plots of the variation of firing rate with membrane area and external current for three different potassium ion channel blockages.

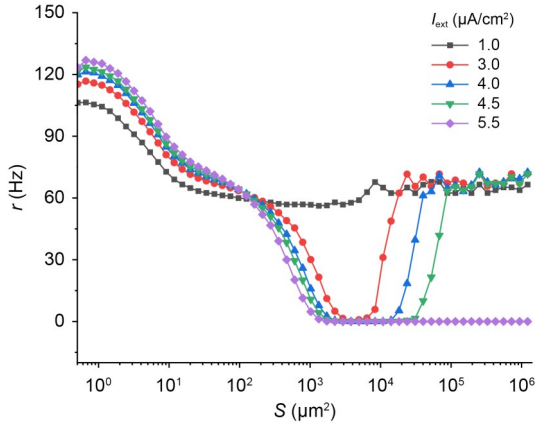

Fig. 5 Mean firing rates of neurons versus noise intensity under different external bias current conditions. The other parameter is set to x_K=0.1

Fig. 6a shows that for x_K=0.10, ISR effects occur in the range of $I_{ext} \in (1.5, 5.5)$ μA/cm^2, and an increase in external current promotes ISR effects. For x_K=0.40, the neuron does not undergo ISR effects (Fig. 6b). For x_K=0.90, the external current for ISR to occur is larger, at approximately $I_{ext} \in (4.5, 5.5)$ μA/cm^2, and an increase in external current suppresses ISR effects (Fig. 6c). Table 1 shows that as I_{ext} increases, the more x_2 is greater than 0.10. As a result, when x_K=0.10, the SFP attractor basin grows as the current does, so an increase in external current promotes the ISR phenomenon and, vice versa, x_3 approaches 0.90 as I_{ext} rises, implying that at x_K=0.90, an increase in current causes the SFP attractor basin to shrink, which in turn suppresses the ISR.

3.2 Inverse stochastic resonance of small-world neuronal networks

ISR in isolated neuronal networks (i.e., where there are no synaptic currents between neurons) is first

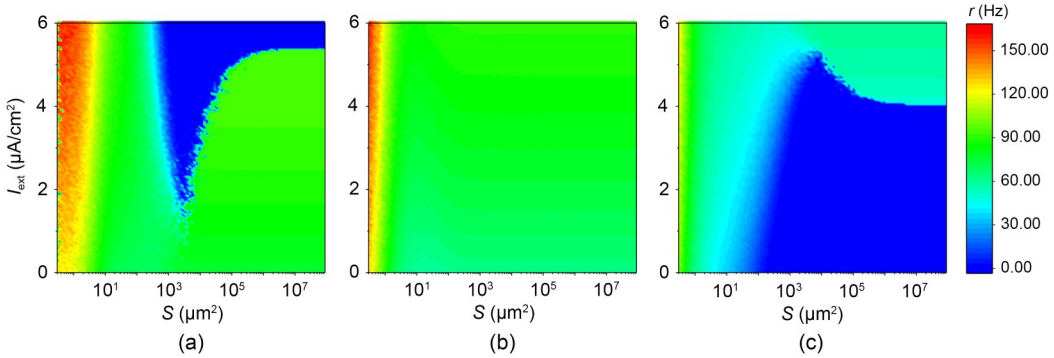

Fig. 6 Contour plots of the average firing rate r in the I_{ext}-S plane at different potassium channel blockage ratios x_K: (a) x_K=0.10; (b) x_K=0.40; (c) x_K=0.90. Note that x_K is negatively correlated with the degree of blockage

discussed. Since the neuronal network is non-uniform in its response to drugs, we use NBR to denote the proportion of neurons in the network with blocked potassium channels to the total number of neurons in the network. To simplify the study process for blocked neurons, we set the top portion of neurons, e.g., NBR=0.2, to the first 20 neurons with potassium channel blockage. The x_K of this part of the neuron is fixed at 0.1 (within the bistable interval). In the following, when calculating the firing rate of the network, each neuron in the network is chosen with the initial values fixed at (−30.08, 0.65, 0.44, 0.44) in the state space (V, m, n, h). Fig. 7a plots the average firing rate of network R versus membrane area for no coupling currents between neurons, for different network blockage ratios NBR. The results indicate that the firing first decreases and then increases with increasing membrane area for different NBRs. The R is zero at moderate intensity of noise. This means that in the isolated neural networks, the ISR phenomenon occurs for different NBRs. In the case of relatively high noise intensity, all neurons in the network are firing, the NBR increases, and the firing rate increases. Figs. 7b and 7c show the firing distribution and spatio-temporal plots, respectively for the network blockage ratios of 60% under small noise. It can be seen that the first 60% of neurons are in a discharging state and the last 40% are in a resting state. Therefore, only bistable neurons in the network are firing at low noise intensities, and the firing rate of the network is positively correlated with the network blockage ratios.

We then explored ISR in the small world network with different electrical coupling strengths g_e. Overall, the ISR is a robust phenomenon across different electrically coupled small-world networks. In Fig. 8a, the ISR was clearly observed under different NBRs. In addition, the membrane area threshold (i.e., the membrane area when the firing rate of the network starts to jump from zero) is different for different NBRs. Fig. 9 shows the threshold versus the NBR in the case where g_e= 0.04 mS/cm^2. The results show that the threshold decreases as NBR increases. This means that the range of noise that can inhibit neuronal firing activity is progressively reduced as the NBR increases. In other words, the increase in the network blockage ratios at small coupling strengths suppresses the ISR effect.

Comparing the right side of Fig. 8a with the middle of Fig. 8b, it can be found that R in the former gradually increases with increasing NBR, while in the latter it changes in the opposite direction. What are the differences in their kinetic mechanisms? As shown in Fig. 8b, the minimum value of the R decreases as the network blocking ratio NBR increases, indicating that the ISR becomes more pronounced with higher NBR. To explain this phenomenon, we use the relative abundance of spiking states (N_s/N) to represent the proportion of neurons in the network that is in the spiking state. The top panel in Fig. 10 represents the N_s/N for three different NBRs, and the bottom panel represents the change in the firing rate of each neuron in the corresponding state. The observation shows that the reason for the decrease in R at moderate noise is that the part of the neuron with potassium channel blockage is resting. So the larger the NBR, the smaller the R of the network under moderate noise. The firing rate of neurons is suppressed to zero due to the 'trapping effect' (Uzuntarla et al., 2017b). In bistable neurons, the SFP and the SLC are divided by the ULC. This boundary is closer to the SLC. Thus, for moderate noise levels, the neuron in the firing state encounters

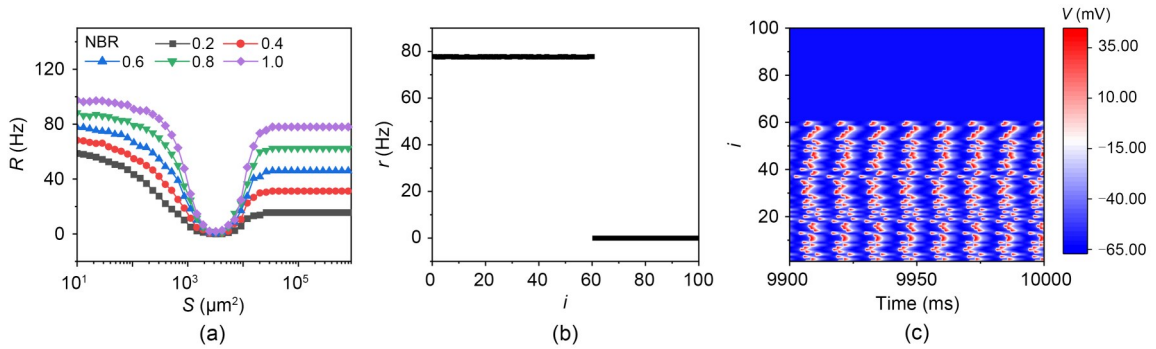

Fig. 7 ISR in isolated neuronal networks: (a) average firing rate of the network as the function of membrane area for different NBRs, with coupling strength g_e=0 mS/cm^2; (b) firing rate of each node in the network under small noise, NBR=0.6 and S=1×10^5 μm^2; (c) spatio-temporal plot in the isolated network under small noise, NBR=0.6 and S=1×10^5 μm^2

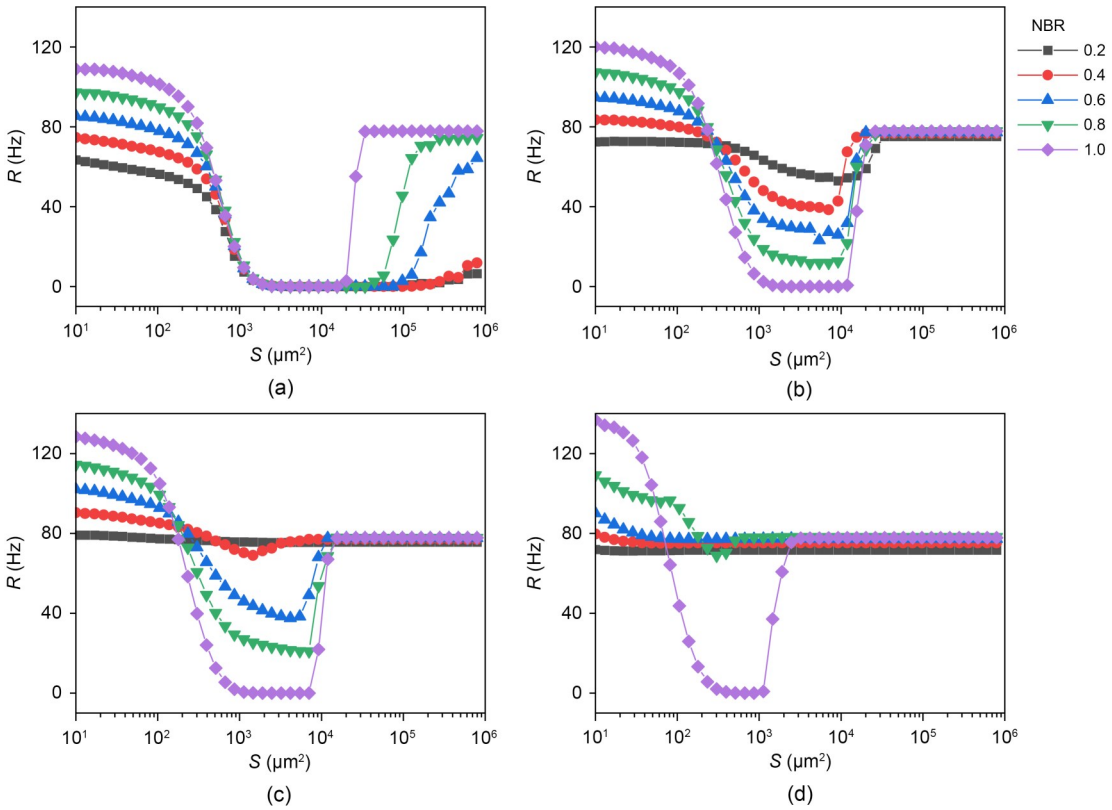

Fig. 8 ISR emergence in the small world network of electrically coupled neurons at different coupling strengths. The average firing rate is the function of membrane area for different coupling strengths g_c: (a) g_c=0.04 mS/cm^2; (b) g_c=0.10 mS/cm^2; (c) g_c=0.17 mS/cm^2; (d) g_c=0.60 mS/cm^2

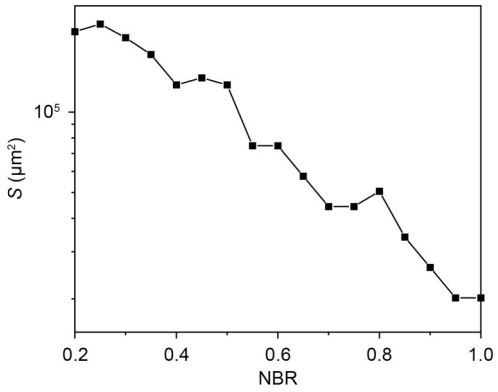

Fig. 9 Relationship between the threshold of membrane area and the network blockage ratio. The threshold refers to the membrane area corresponding to the jump of *R* from zero, with g_c=0.04 mS/cm^2

a noise kick that causes it to cross the boundary and enter the basin of the SFP where it is captured. Once captured, the neuron will gradually became resting and have difficulty in being returned to the SLC. To sum up, under moderate noise intensity *R* becomes smaller because the noise suppresses the firing of bistable neurons. The more the number of bistable neurons in the network, the more pronounced the suppression of the firing rate of the network.

Fig. 8c represents the *R* versus membrane area for different NBRs for the coupling strength g_c=0.17 mS/cm^2. There is no significant ISR phenomenon on the network when NBR=0.2. Comparing Fig. 8b and Fig. 8c, we find that for the same NBR, an increase in coupling strength results in a greater minimum value of the curve. This is because the SFP of the bistable neuron (Fig. 11 green dot) is outside the excited trajectory of the monostable neuron (Fig. 11 blue trajectory), such that a potential difference will form between the bistable neuron in the resting state and the monostable neuron in the firing state. When the coupling strength becomes greater, it leads to a greater synaptic current in the bistable neuron, and the neuron discharges steadily as a result. That can be confirmed in Figs. 12a and 12b; when the coupling strength increases, the bistable neuron will be pulled to the limit circle in a firing state. This effect diminishes when the number of monostable firing neurons decreases. In Fig. 12a, the ratio of

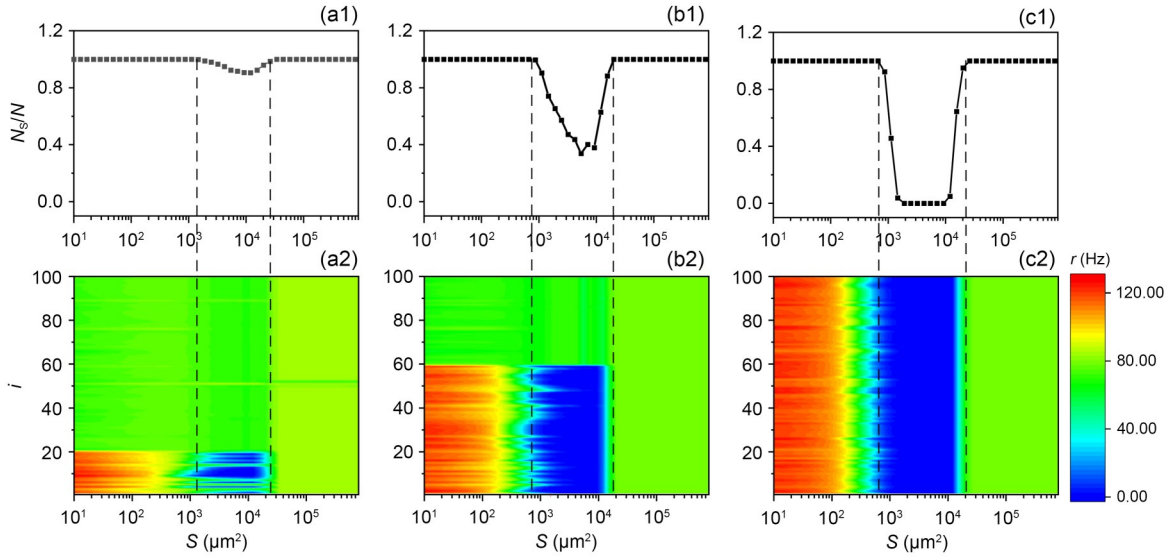

Fig. 10 Firing behavior of neurons at different ratios of network blockage. g_e=0.10 mS/cm², top panel is the relative abundance N_s/N of neurons in the firing state, and bottom panel is the firing rate of each neuron in the network as a function of membrane area. (a1 and a2) NBR=0.2; (b1 and b2) NBR=0.6; (c1 and c2) NBR=1.0

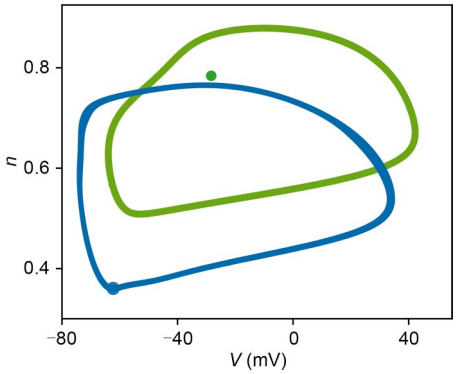

Fig. 11 Phase diagrams of bistable and monostable neurons in the (V, n) plane. Green indicates SFP and SLC for the bistable neurons, and blue indicates resting state and stimulated trajectory for the monostable neurons. I_{ext}= 4.0 μA/cm². Reference to color refers to the online version of this figure

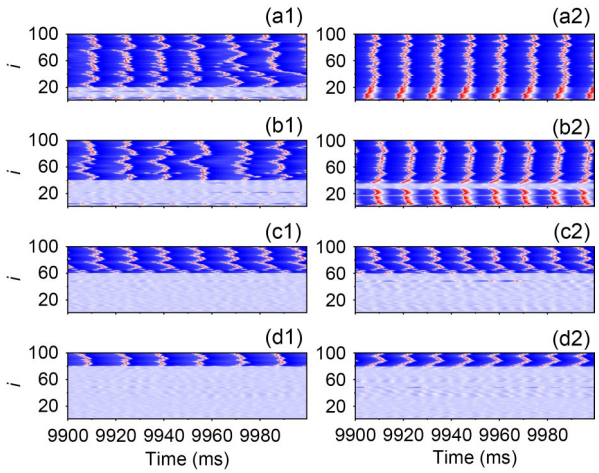

Fig. 12 Behaviour of neurons in the network with different coupling strengths and network blockage ratios. S=4000 μm², for left column g_e=0.1 mS/cm², and for right column g_e= 0.17 mS/cm². (a1 and a2) NBR=0.2; (b1 and b2) NBR=0.4; (c1 and c2) NBR=0.6; (d1 and d2) NBR=0.8

the number of monostable to bistable neurons is 8:2, 20% of all bistable neurons firing for g_e=0.17 mS/cm². However, in Fig. 12b2, there are some bistable neurons that remain in the resting state. There is little difference in the firing states of the neurons between Fig. 12c and Fig. 12d. Due to this effect, an increase in coupling strength suppresses ISR. Fig. 8d indicates that significant ISR only occurs at NBR=0.8 and 1.0 for coupling strength g_e=0.6 mS/cm². Thus, as long as there is a potential difference between monostable and bistable neurons, a strong coupling current will override any effect that noise may have, given a sufficiently high coupling strength. So an increase in coupling strength will suppress ISR.

In addition, the ISR phenomenon occurs regardless of the coupling strength and the firing rate is suppressed to zero when the NBR is 100%. Because each neuron in the network is a bistable neuron, there is no monostable neuron to pull a bistable neuron from the stable fixed point to the limit circle. Each neuron has the potential to undergo ISR, and firing rates of neurons are all suppressed to zero at moderate noise intensities.

The minimum firing rate of the network with respect to the NBR at different coupling strengths is shown in Fig. 13. It shows that at smaller coupling strengths g_e=0.04 mS/cm^2, the minimum value of the network firing rate is zero regardless of the NBR. This means that ISR will occur in small coupled neuronal networks regardless of the NBR. Comparing the two curves for coupling strengths of 0.17 and 0.60 mS/cm^2, it can be seen that, as the coupling strength increases, the range of NBR that can generate ISR appearances gradually decreases. For NBR=1.0, the ISR occurs, and the minimum firing rate is zero. Moreover, we also observed that the threshold for the minimum NBR that can occur with ISR increases as the coupling strength increases, because in the case of moderate noise, the noise kicks the bistable neuron from the limit cycle to the stable equilibrium, whereas a sufficiently large coupling current gives a stimulus to return it to the limit cycles. The higher the coupling current, the less the network firing rate decreases for a given network blocking ratio, so that the increasing coupling strength counteracts the trapping effect.

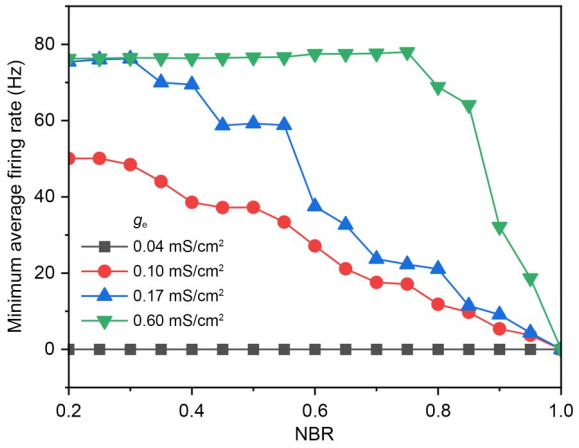

Fig. 13 Minimum value of the average firing rate relative to the NBRs in different electrically coupled neuronal networks

To further investigate the relationship between the average firing rate R and the coupling strength g_e, Fig. 14 shows the response of the firing rate of the network to the coupling strength at different noise intensities. As shown in Fig. 14a, for a noise intensity of S=1000 μm^2, R first decreases slowly to a minimum or remains constant and then increases rapidly as g_e gradually increases. However, for NBR=0.2 and NBR=0.4, there is no significant minimum value. Fig. 14b shows the variation of the average firing rate with coupling strength for a noise intensity of S=3000 μm^2. The observation shows that for different NBRs, the average firing rate of the network increases rapidly from zero as the coupling strength increases. In addition, the threshold of the coupling strength for this shift increases as the NBR increases. In both plots in Fig. 14, the curves have a rapid rise and then fall in common. We explored the reasons for this phenomenon.

Two conditions are required for a bistable neuron to fire under moderate intensity noise: a sufficiently large coupling strength and a potential difference between it and the monostable neurons. Therefore, for the network's firing rate increasing from zero, we analyzed and reasonably speculated that the network's firing rate first increased because the monostable neurons were first in the firing state. Afterwards there would be a potential difference between the monostable and bistable neurons, due to the increase in coupling strength,

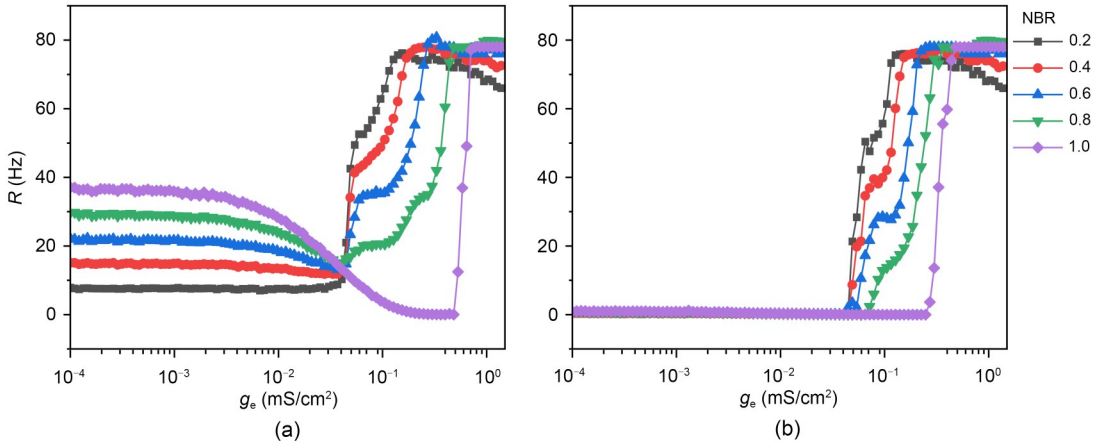

Fig. 14 Average firing rate of the network with coupling strength for moderate noise intensity: (a) S=1000 μm^2; (b) S=3000 μm^2

for the bistable neurons to be pulled into the firing state. Fig. 15 confirms our speculation. We take Fig. 14a (NBR=0.6) as an example, Fig. 15 shows the distribution of firing at three coupling strengths during the period of increasing network firing rate. It can be seen that first the monostable neurons fire, then the number of bistable neurons in the firing state gradually increases with increasing coupling strength.

It is worth noting that in Fig. 14, except for NBR=1.0, the firing rate of the network reaches a maximum and then gradually decreases. Taking Fig. 14b as an example, the NBRs are 0.2 and 1.0, and the spatio-temporal plot and firing distribution at large coupling strength g_e=1.0 mS/cm^2 are shown in Fig. 16. We know that the firing rate of neurons with NBR=1.0 is greater than that of neurons with NBR=0.2 firing rate. This is because, at large coupling strengths, the neuronal networks are all in a discharge-synchronous state and the firing rates are all close to the natural firing rates. However, on the one hand, there is heterogeneity between bistable and monostable neurons in which the eigenfrequencies of the two are not the same while, on the other hand, electrical coupling is connecting neurons throughout the discharge process and thus the membrane potential difference that always exists between neurons will coordinate the discharge frequencies with each other. So the overall firing rate of the network is smaller than the natural discharge rate, and the more bistable neurons there are, the larger is the network discharge rate.

4 Conclusions

Previous studies have shown that the ISR induced by a variety of factors is widespread in single neurons and neuronal networks (Uzuntarla, 2013; Uzuntarla et al., 2013, 2017b). Certain drugs can affect neuronal information transfer processes by causing ion channel inactivation (Narahashi and Moore, 1968; Hoyt and Strieb, 1971). Currently, the effect of potassium channel blockage on ISR in HH neural systems has not received much attention.

In this paper, we focused on the effect of potassium ion channel blockage on ISR in HH neural systems.

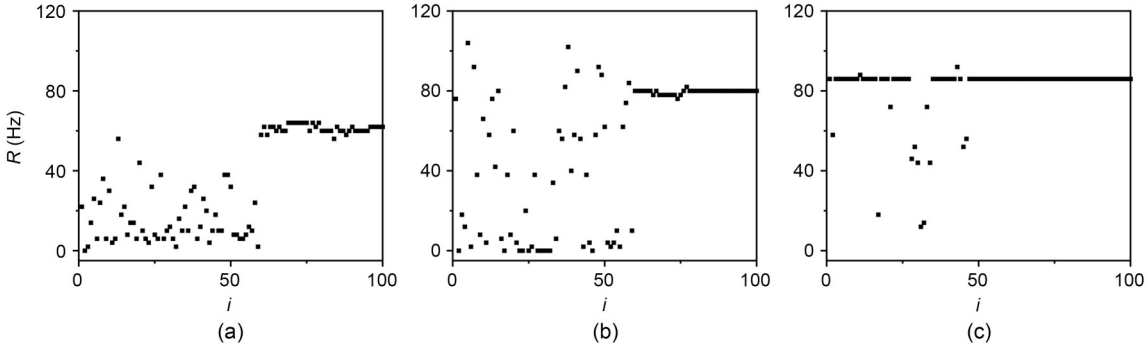

Fig. 15 Effect of coupling strength on the firing rate of neurons in small-world networks on moderate noise intensity (S=1000 μm^2, NBR=0.6): (a) g_e=0.08 mS/cm^2; (b) g_e=0.20 mS/cm^2; (c) g_e=0.30 mS/cm^2

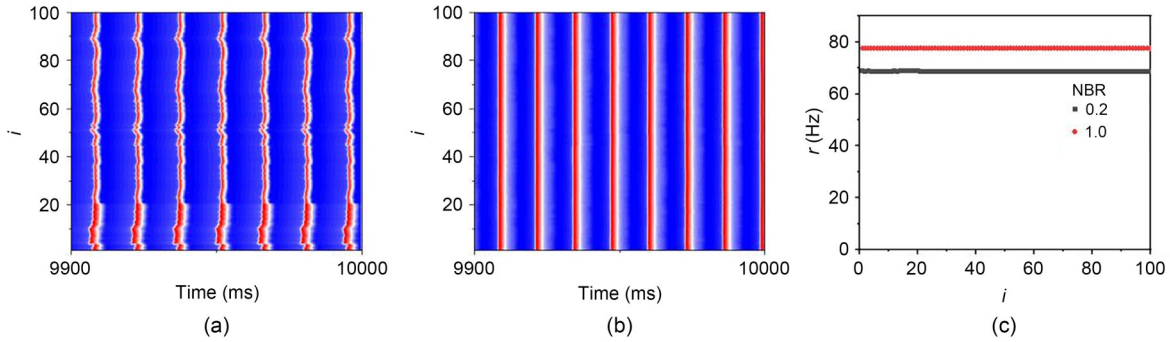

Fig. 16 Effect of network blocking ratio on neuronal firing in small-world networks on moderate noise intensity. Spatio-temporal plots for two different network blockage ratios of NBR=0.2 (a) and NBR=1.0 (b) with g_e=1.0 mS/cm^2 and S=3000 μm^2; (c) is the firing distribution corresponding to (a) and (b)

The results show that in single neurons, ion channel noise-induced ISR effects can occur only at a certain small range of potassium channel blockage ratios. The bifurcation analysis showed that within this small range is the bistable region, where stable fixed point and stable limit cycles coexist, and this range is regulated by the external bias current. Therefore, the bistable kinetic structure of HH neurons and external noise are necessary for the generation of ISR.

We further investigated the ISR effect in small-world networks. Since drug effects are non-uniform across neurons in the network, we introduced the network blockage ratio NBR, which is the ratio of neurons with potassium channel blockage in the network to the total neurons in the network. At small coupling strengths, an increase in NBR resulted in shorter ISR durations. When the coupling strength is increased, the ISR was more pronounced in the case of large NBR. The reason for the presence of ISR is that the firing of bistable neurons is inhibited at moderate levels of noise. However, when there is a potential difference between the bistable and monostable neurons and the coupling strength is increased, this inhibition is counteracted. In summary, the appearance of ISR depends on the interaction of the network blockage ratios, the coupling strength, and the ion channel noise.

Previous studies have shown that ISR has been observed in individual Purkinje cells of the rat brain (Buchin et al., 2016), suggesting that the necessary kinetic structures for ISR to occur are present in biological individuals. Thus, ISR can be used to improve biological function. For example, the transmission of locally optimal information during cerebellar information processing (Buchin et al., 2016), the suppression of specific bands in working memory (Dipoppa and Gutkin, 2013), and the stochastic facilitation effect in auditory brain stem cells (Schmerl and McDonnell, 2013). In addition, ISR can be used to filter irrelevant information, thus allowing the nervous system to process information more selectively. In this paper, we have only considered ISR in small-world networks with electrically coupled connections. However, the phenomenon of ISR in more realistic neuronal (Ma et al., 2019) network structures as well as in connection patterns remains to be explored. Examples include neural networks in the cerebral cortex that are connected by the balance of excitatory and inhibitory synapses (Shu et al., 2003; Heiss et al., 2008).

Acknowledgments

This work is supported by the National Natural Science Foundation of China (No. 12175080) and the Fundamental Research Funds for the Central Universities (No. CCNU22JC009), China.

Author contributions

Xueqing WANG and Dong YU designed the research. Xueqing WANG and Dong YU processed the corresponding data. Xueqing WANG wrote the first draft of the manuscript. Yong WU, Tianyu LI, and Qianming DING helped to organize the manuscript. Dong YU and Ya JIA revised and edited the final version.

Conflict of interest

Xueqing WANG, Dong YU, Yong WU, Qianming DING, Tianyu LI, and Ya JIA declare that they have no conflict of interest.

References

Buchin A, Rieubland S, Häusser M, et al., 2016. Inverse stochastic resonance in cerebellar Purkinje cells. *PLoS Computational Biology*, 12(8):e1005000. https://doi.org/10.1371/journal.pcbi.1005000

Chik DTW, Wang YQ, Wang ZD, 2001. Stochastic resonance in a Hodgkin-Huxley neuron in the absence of external noise. *Physical Review E*, 64(2):021913. https://doi.org/10.1103/PhysRevE.64.021913

Ding QM, Jia Y, 2021. Effects of temperature and ion channel blocks on propagation of action potential in myelinated axons. *Chaos: An Interdisciplinary Journal of Nonlinear Science*, 31(5):053102. https://doi.org/10.1063/5.0044874

Dipoppa M, Gutkin BS, 2013. Flexible frequency control of cortical oscillations enables computations required for working memory. *Proceedings of the National Academy of Sciences of the United States of America*, 110(31): 12828-12833. https://doi.org/10.1073/pnas.1303270110

Faisal AA, Selen LPJ, Wolpert DM, 2008. Noise in the nervous system. *Nature Reviews Neuroscience*, 9(4):292-303. https://doi.org/10.1038/nrn2258

Fox RF, 1997. Stochastic versions of the Hodgkin-Huxley equations. *Biophysical Journal*, 72(5):2068-2074. https://doi.org/10.1016/S0006-3495(97)78850-7

Gailey PC, Neiman A, Collins JJ, et al., 1997. Stochastic resonance in ensembles of nondynamical elements: the role of internal noise. *Physical Review Letters*, 79(23):4701-4704. https://doi.org/10.1103/PhysRevLett.79.4701

Gluckman BJ, Netoff TI, Neel EJ, et al., 1996. Stochastic resonance in a neuronal network from mammalian brain. *Physical Review Letters*, 77(19):4098-4101. https://doi.org/10.1103/PhysRevLett.77.4098

Goldwyn JH, Imennov NS, Famulare M, et al., 2011. Stochastic differential equation models for ion channel noise

in Hodgkin–Huxley neurons. *Physical Review E*, 83(4): 041908.
https://doi.org/10.1103/PhysRevE.83.041908

Gutkin BS, Jost J, Tuckwell HC, 2009. Inhibition of rhythmic neural spiking by noise: the occurrence of a minimum in activity with increasing noise. *Naturwissenschaften*, 96(9): 1091-1097.
https://doi.org/10.1007/s00114-009-0570-5

Heiss JE, Katz Y, Ganmor E, et al., 2008. Shift in the balance between excitation and inhibition during sensory adaptation of S1 neurons. *Journal of Neuroscience*, 28(49):13320-13330.
https://doi.org/10.1523/JNEUROSCI.2646-08.2008

Hodgkin AL, Huxley AF, 1952a. The dual effect of membrane potential on sodium conductance in the giant axon of *Loligo*. *The Journal of Physiology*, 116(4):497-506.
https://doi.org/10.1113/jphysiol.1952.sp004719

Hodgkin AL, Huxley AF, 1952b. A quantitative description of membrane current and its application to conduction and excitation in nerve. *The Journal of Physiology*, 117(4): 500-544.
https://doi.org/10.1113/jphysiol.1952.sp004764

Hoyt RC, Strieb JD, 1971. A stored charge model for the sodium channel. *Biophysical Journal*, 11(11):868-885.
https://doi.org/10.1016/S0006-3495(71)86261-6

Huh JH, 2016. Inverse stochastic resonance in electroconvection by multiplicative colored noise. *Physical Review E*, 94(5):052702.
https://doi.org/10.1103/PhysRevE.94.052702

Jin WY, Wang A, Ma J, et al., 2019. Effects of electromagnetic induction and noise on the regulation of sleep wake cycle. *Science China Technological Sciences*, 62(12):2113-2119.
https://doi.org/10.1007/s11431-018-9423-x

Kawaguchi M, Mino H, Durand DM, 2011. Stochastic resonance can enhance information transmission in neural networks. *IEEE Transactions on Biomedical Engineering*, 58(7):1950-1958.
https://doi.org/10.1109/TBME.2011.2126571

Kosko B, Mitaim S, 2003. Stochastic resonance in noisy threshold neurons. *Neural Networks*, 16(5-6):755-761.
https://doi.org/10.1016/S0893-6080(03)00128-X

Li DX, Cui XW, Yang YC, 2018. Inverse stochastic resonance induced by non-Gaussian colored noise. *Neurocomputing*, 287:52-57.
https://doi.org/10.1016/j.neucom.2018.01.078

Li DX, Song SL, Zhang N, 2020. Lévy noise-induced inverse stochastic resonance on Newman–Watts networks of Hodgkin–Huxley neurons. *International Journal of Modern Physics B*, 34(19):2050185.
https://doi.org/10.1142/S0217979220501854

Liu SB, Wu Y, Li JJ, et al., 2013. The dynamic behavior of spiral waves in stochastic Hodgkin–Huxley neuronal networks with ion channel blocks. *Nonlinear Dynamics*, 73(1-2):1055-1063.
https://doi.org/10.1007/s11071-013-0852-5

Liu Y, Li CG, 2013. Stochastic resonance in feedforward-loop neuronal network motifs in astrocyte field. *Journal of Theoretical Biology*, 335:265-275.
https://doi.org/10.1016/j.jtbi.2013.07.007

Liu Y, Ma J, Xu Y, et al., 2019. Electrical mode transition of hybrid neuronal model induced by external stimulus and electromagnetic induction. *International Journal of Bifurcation and Chaos*, 29(11):1950156.
https://doi.org/10.1142/S0218127419501566

Lu LL, Jia Y, Liu WH, et al., 2017. Mixed stimulus-induced mode selection in neural activity driven by high and low frequency current under electromagnetic radiation. *Complexity*, 2017:7628537.
https://doi.org/10.1155/2017/7628537

Lu LL, Jia Y, Ge MY, et al., 2020. Inverse stochastic resonance in Hodgkin–Huxley neural system driven by Gaussian and non-Gaussian colored noises. *Nonlinear Dynamics*, 100(1):877-889.
https://doi.org/10.1007/s11071-020-05492-y

Ma J, 2023. Biophysical neurons, energy, and synapse controllability: a review. *Journal of Zhejiang University-SCIENCE A (Applied Physics & Engineering)*, 24(2):109-129.
https://doi.org/10.1631/jzus.A2200469

Ma J, Wu Y, Ying HP, et al., 2011. Channel noise-induced phase transition of spiral wave in networks of Hodgkin-Huxley neurons. *Chinese Science Bulletin*, 56(2):151-157.
https://doi.org/10.1007/s11434-010-4281-2

Ma J, Yang ZQ, Yang LJ, et al., 2019. A physical view of computational neurodynamics. *Journal of Zhejiang University-SCIENCE A (Applied Physics & Engineering)*, 20(9):639-659.
https://doi.org/10.1631/jzus.A1900273

Maisel B, Lindenberg K, 2020. Channel noise effects on neural synchronization. *Physica A: Statistical Mechanics and Its Applications*, 552:123186.
https://doi.org/10.1016/j.physa.2019.123186

McDonnell MD, Abbott D, 2009. What is stochastic resonance? Definitions, misconceptions, debates, and its relevance to biology. *PLoS Computational Biology*, 5(5):e1000348.
https://doi.org/10.1371/journal.pcbi.1000348

Narahashi T, Moore JW, 1968. Neuroactive agents and nerve membrane conductances. *Journal of General Physiology*, 51(5):93-101.
https://doi.org/10.1085/jgp.51.5.93

Paydarfar D, Forger DB, Clay JR, 2006. Noisy inputs and the induction of on–off switching behavior in a neuronal pacemaker. *Journal of Neurophysiology*, 96(6):3338-3348.
https://doi.org/10.1152/jn.00486.2006

Perc M, 2007. Stochastic resonance on excitable small-world networks via a pacemaker. *Physical Review E*, 76(6):066203.
https://doi.org/10.1103/PhysRevE.76.066203

Schmerl BA, McDonnell MD, 2013. Channel-noise-induced stochastic facilitation in an auditory brainstem neuron model. *Physical Review E*, 88(5):052722.
https://doi.org/10.1103/PhysRevE.88.052722

Schmid G, Goychuk I, Hänggi P, 2004. Effect of channel block on the spiking activity of excitable membranes in a stochastic Hodgkin–Huxley model. *Physical Biology*, 1(2): 61-66.
https://doi.org/10.1088/1478-3967/1/2/002

Shu YS, Hasenstaub A, McCormick DA, 2003. Turning on and off recurrent balanced cortical activity. *Nature*, 423(6937): 288-293.
https://doi.org/10.1038/nature01616

Tuckwell HC, Jost J, Gutkin BS, 2009. Inhibition and modulation of rhythmic neuronal spiking by noise. *Physical Review E*, 80(3):031907.
https://doi.org/10.1103/PhysRevE.80.031907

Uzun R, Yilmaz E, Ozer M, 2017. Effects of autapse and ion channel block on the collective firing activity of Newman–Watts small-world neuronal networks. *Physica A: Statistical Mechanics and Its Applications*, 486:386-396.
https://doi.org/10.1016/j.physa.2017.05.049

Uzuntarla M, 2013. Inverse stochastic resonance induced by synaptic background activity with unreliable synapses. *Physics Letters A*, 377(38):2585-2589.
https://doi.org/10.1016/j.physleta.2013.08.009

Uzuntarla M, Cressman JR, Ozer M, et al., 2013. Dynamical structure underlying inverse stochastic resonance and its implications. *Physical Review E*, 88(4):042712.
https://doi.org/10.1103/PhysRevE.88.042712

Uzuntarla M, Torres JJ, So P, et al., 2017a. Double inverse stochastic resonance with dynamic synapses. *Physical Review E*, 95(1):012404.
https://doi.org/10.1103/PhysRevE.95.012404

Uzuntarla M, Barreto E, Torres JJ, 2017b. Inverse stochastic resonance in networks of spiking neurons. *PLoS Computational Biology*, 13(7):e1005646.
https://doi.org/10.1371/journal.pcbi.1005646

Wang GW, Wu Y, Xiao FL, et al., 2022. Non-Gaussian noise and autapse-induced inverse stochastic resonance in bistable Izhikevich neural system under electromagnetic induction. *Physica A: Statistical Mechanics and Its Applications*, 598: 127274.
https://doi.org/10.1016/j.physa.2022.127274

Wang QY, Perc M, Duan ZS, et al., 2009. Delay-induced multiple stochastic resonances on scale-free neuronal networks. *Chaos: An Interdisciplinary Journal of Nonlinear Science*, 19(2):023112.
https://doi.org/10.1063/1.3133126

Watts DJ, Strogatz SH, 1998. Collective dynamics of 'small-world' networks. *Nature*, 393(6684):440-442.
https://doi.org/10.1038/30918

White JA, Rubinstein JT, Kay AR, 2000. Channel noise in neurons. *Trends in Neurosciences*, 23(3):131-137.
https://doi.org/10.1016/S0166-2236(99)01521-0

Wu FQ, Ma J, Ren GD, 2018. Synchronization stability between initial-dependent oscillators with periodical and chaotic oscillation. *Journal of Zhejiang University-SCIENCE A (Applied Physics & Engineering)*, 19(12):889-903.
https://doi.org/10.1631/jzus.A1800334

Wu XY, Ma J, Li F, et al., 2013a. Development of spiral wave in a regular network of excitatory neurons due to stochastic poisoning of ion channels. *Communications in Nonlinear Science and Numerical Simulation*, 18(12):3350-3364.
https://doi.org/10.1016/j.cnsns.2013.05.011

Wu XY, Ma J, Xie ZB, 2013b. Effect of inhomogeneous distribution of ion channels on collective electric activities of neurons in a ring network. *Acta Physica Sinica*, 62(24): 240507 (in Chinese).
https://doi.org/10.7498/aps.62.240507

Xu Y, Jia Y, Ge MY, et al., 2018. Effects of ion channel blocks on electrical activity of stochastic Hodgkin–Huxley neural network under electromagnetic induction. *Neurocomputing*, 283:196-204.
https://doi.org/10.1016/j.neucom.2017.12.036

Xu Y, Jia Y, Wang HW, et al., 2019. Spiking activities in chain neural network driven by channel noise with field coupling. *Nonlinear Dynamics*, 95(4):3237-3247.
https://doi.org/10.1007/s11071-018-04752-2

Yu D, Lu LL, Wang GW, et al., 2021. Synchronization mode transition induced by bounded noise in multiple time-delays coupled FitzHugh–Nagumo model. *Chaos, Solitons & Fractals*, 147:111000.
https://doi.org/10.1016/j.chaos.2021.111000

Yu D, Wang GW, Ding QM, et al., 2022a. Effects of bounded noise and time delay on signal transmission in excitable neural networks. *Chaos, Solitons & Fractals*, 157:111929.
https://doi.org/10.1016/j.chaos.2022.111929

Yu D, Zhou XY, Wang GW, et al., 2022b. Effects of chaotic activity and time delay on signal transmission in FitzHugh-Nagumo neuronal system. *Cognitive Neurodynamics*, 16(4): 887-897.
https://doi.org/10.1007/s11571-021-09743-5

Yu D, Wu Y, Ye ZQ, et al., 2022c. Inverse chaotic resonance in Hodgkin–Huxley neuronal system. *The European Physical Journal Special Topics*, 231(22-23):4097-4107.
https://doi.org/10.1140/epjs/s11734-022-00629-z

Yu D, Wu Y, Yang LJ, et al., 2023a. Effect of topology on delay-induced multiple resonances in locally driven systems. *Physica A: Statistical Mechanics and Its Applications*, 609: 128330.
https://doi.org/10.1016/j.physa.2022.128330

Yu D, Wang GW, Li TY, et al., 2023b. Filtering properties of Hodgkin-Huxley neuron on different time-scale signals. *Communications in Nonlinear Science and Numerical Simulation*, 117:106894.
https://doi.org/10.1016/j.cnsns.2022.106894

Zhang XF, Ma J, 2021. Wave filtering and firing modes in a light-sensitive neural circuit. *Journal of Zhejiang University-SCIENCE A (Applied Physics & Engineering)*, 22(9):707-720.
https://doi.org/10.1631/jzus.A2100323

Zhao Y, Li DX, 2019. Levy noise-induced inverse stochastic resonance in a single neuron. *Modern Physics Letters B*, 33(21):1950252.
https://doi.org/10.1142/S021798491950252X

Zhou XY, Xu Y, Wang GW, et al., 2020. Ionic channel blockage in stochastic Hodgkin–Huxley neuronal model driven by multiple oscillatory signals. *Cognitive Neurodynamics*, 14(4):569-578.
https://doi.org/10.1007/s11571-020-09593-7